# Conversion of surface carbidic to subsurface carbon on cobalt (0001) - a theoretical-study

Surface Science 240 (1990) 253–262
North-Holland



# Conversion of surface carbidic to subsurface carbon on cobalt (0001): a theoretical study

M.C. Zonnevylle, J.J.C. Geerlings
*Koninklijke / Shell-Laboratorium, Amsterdam (Shell Research B.V.), Badhuisweg 3, 1031 CM Amsterdam, Netherlands*

and

R.A. van Santen
*Laboratory of Inorganic Chemistry and Catalysis, Technical University of Eindhoven, P.O. Box 513, 5600 MB Eindhoven, Netherlands*

Received 5 June 1990; accepted for publication 10 August 1990

Preliminary HFS–LCAO calculations of a nine atom cobalt cluster reveal a minimal energy difference between surface carbidic and subsurface carbon configurations. The electron withdrawing power, and therefore the poisoning effect on potential CO adsorption, is maximal for subsurface C, but localized to immediately neighboring metal atoms. If the metal lattice is kept fixed, the barrier for moving the carbon atom between the two sites is high (4.70 eV) because of steric repulsion. If the three-fold hollow of the cobalt cluster is stretched slightly by only 1%, the barrier is reduced by nearly 50%. By analogy to effective medium calculations, we may expect thermally active phonon modes to allow as much as a 10% lattice relaxation, which can reduce the surface to subsurface carbon barrier by 90% (0.49 eV). Coadsorption with oxygen favors the subsurface carbon site.

## 1. Introduction

Under heterogeneous catalysis conditions, an accurate characterization of the important surface(s) at an atomic level is extremely difficult. Surface scientists have more success working with single crystal samples under UHV conditions. But again, circumstances often arise which hinder full characterization. A particularly difficult, yet important, example is the occurrence of subsurface atomic species. In metals, such species can modify the electronic properties of the surface such that it may (locally) exhibit qualities more closely resembling a semiconductor (or insulator) than a metal. The shift in surface makeup can strongly influence ongoing reactions. If adatoms are known to form under a particular set of reaction conditions, it is difficult to rule out the formation of subsurface species by "classical" UHV techniques.

One important case is the formation of subsurface carbon. It is a potential problem under any reaction condition which creates atomic carbon as either a transient surface species or as a final product. A clear example is the Fischer–Tropsch process, in which CO and $H_2$ are converted to various hydrocarbons. It is now widely accepted that the first step in the reaction is the cleavage of carbon monoxide to form specifically surface carbidic, rather than graphitic, carbon [1] and oxygen. The latter is removed from the surface through the formation of gaseous $H_2O$, and $CO_2$ in the case of Fe. The carbon, if it remains in the carbidic rather than graphitic form, is hydrogenated [2], and continues on to form hydrocarbons. Graphitic carbon appears essentially unreactive under hydrogenation conditions.

The correspondence between the ability of a transition metal to dissociate CO and the stability

of its bulk carbide has been previously noted [1b,3]. However, it remains unclear whether this parallel is of any consequence in the Fischer–Tropsch process. To our knowledge, only in the case of Fe has the formation of a bulk carbide (primarily $Fe_5C_2$, the Hägg carbide) been observed during the reaction [4]. Certainly, precipitation of graphitic carbon from bulk carbides, e.g., cobalt carbides [5], and carbon-doped transition metal surface [6] has long been known to occur, although at higher temperatures. In the light of this correspondence, the conversion from surface carbidic carbon to subsurface carbon becomes an interesting possibility.

As part of our ongoing investigation of the Fischer–Tropsch reaction over cobalt single crystals [7], we will use the local density functional (LDF) approach to focus specifically on the formation of subsurface carbon in metallic cobalt. Because theoretical investigations of similar processes are uncommon, and the applicability of LDF methods is in this case unclear, we have restricted ourselves to a treatment of small clusters, without geometry optimalization. A more rigorous study at this point will generate a computational effort inappropriate to the preliminary nature of the present work. However, to examine the effects of subsurface species on the adsorption and reactivity characteristics of the metal surface directly, we plan to perform more extensive calculations in the future.

## 2. Method

The Hartree–Fock–Slater LCAO discrete variational methodology [8] has been used to model a variety of surface-adsorbate systems [9]. Naturally one must keep in mind the limitations of using a cluster of finite size to represent the metal surface. In the case of s-metals, such as Cu and Ag, the cluster size may be very large. For example, a 24-atom Ag cluster was used by van den Hoek et al. [9a]. But even in this case, 14 of the atoms had a frozen 4d valence shell, in addition to the frozen core orbitals employed for the remaining 10 atoms. The $d^7s^2$ configuration of cobalt is more problematic; not only is it impossible to use a frozen d

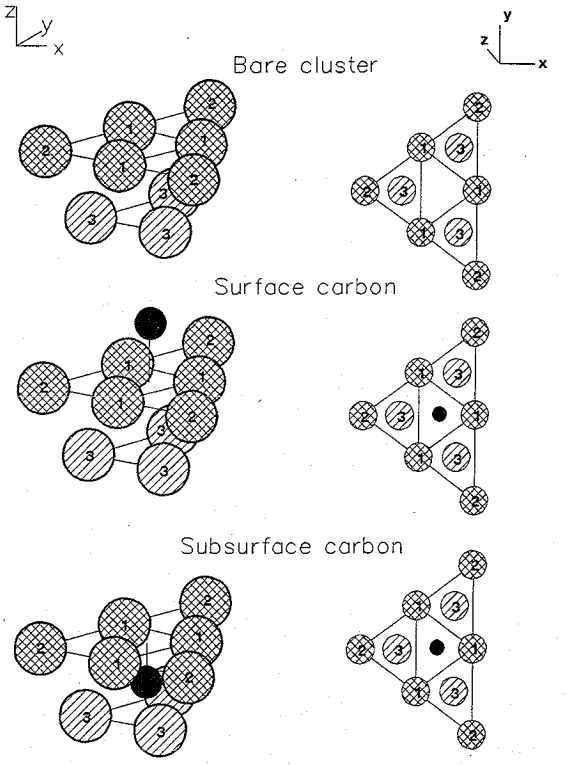


Fig. 1. Geometry of bare $Co_9$ cluster and surface and subsurface carbon models.

valence shell, but achieving convergence is also more difficult.

To model both the surface and octahedral subsurface sites of the the hexagonal close-packed (0001) surface, the nine atom cluster of cobalt depicted in fig. 1 has been selected. Six atoms form the top layer, and three the second layer. Both the three-fold hollow surface and octahedral subsurface sites are provided with their full coordination sphere. The next larger cluster of $C_{3v}$ symmetry contains three additional bottom layer cobalt atoms. Because of the preliminary nature of this study, we have chosen for the smaller cluster. The local $X_\alpha$ ($\alpha = 0.70$) exchange functional was used. The Slater type orbital (STO) basis sets are listed in table 1 [10], and are of double zeta quality. For Co, all core orbitals up to 3p were frozen. For C and O, the 1s orbital is kept frozen. Polarization fit functions have been added.

It is difficult to devise an absolute scale by which a cluster of finite size can be judged "large

Table 1
Exponential coefficients for basis functions

| Co | | C | | O | |
|---|---|---|---|---|---|
| 1s [a] | 14.10 | 1s [a] | 5.40 | 1s [a] | 7.36 |
| 2s [a] | 11.65 | 2s | 1.24 | 2s | 1.70 |
| 3s [a] | 4.85 | 2s | 1.98 | 2s | 2.82 |
| 2p [a] | 10.74 | 2p | 0.96 | 2p | 1.30 |
| 3p [a] | 4.18 | 2p | 2.20 | 2p | 3.06 |
| 3d | 1.50 | 3d | 2.50 | 3d | 2.00 |
| 3d | 3.25 | | | | |
| 3d | 6.70 | | | | |
| 4s | 0.85 | | | | |
| 4s | 1.40 | | | | |
| 4s | 2.40 | | | | |
| 4p | 1.43 | | | | |

[a] Additional functions for core orthogonalization.

enough" to properly represent a metallic surface. Certain calculated properties, such as binding energy, are well known to oscillate with cluster size [11]. Consider the previously mentioned 4-, 10- and 24-atom Ag clusters [9a]; the structure of the d band closely resembles the bulk even for the smallest clusters, but the very disperse s band shows unphysical oscillations even in the 24-atom cluster. However, the work provides evidence that, although absolute values of calculated properties are incorrect, the important trends are properly modelled by the cluster calculations.

We consider two main criteria to judge the cluster size: first, the extent of charge localization. The net atomic charge of an ideal bulk metal sample is zero, differing only slightly in the first few surface layers. The nine-atom cobalt cluster exhibits very little charge localization; the maximum is $-0.0046\ e^-$ on Co(2). However, as this result may be fortuitous, the second, and more important consideration, is for the electronic structure of the cluster: does it resemble that of a metal? Three subcriteria are examined.

First, as the Fermi level of a transition metal cuts through the dense band of spatially delocalized d states, the gap between the highest occupied molecular orbital (HOMO) and the lowest unoccupied molecular orbital (LUMO) should be small. Our computed gap for the $Co_9$ cluster is in fact so small that proper convergence of the ground electronic state $(10(a_1)^2\ 4(a_2)^2\ 13(e)^2\ 14(e)^{0.5})$ is difficult to obtain. The ground state of similar clusters (i.e., few metal atoms) is often characterized by partial occupation of a number of levels, analogous to the partial occupation of crystal orbitals which cut across the Fermi level of a bulk metal. Even with our use of fractional occupation numbers, a true ground state, which explicitly follows the aufbau principle is difficult to find computationally, as this state lies very close in energy to a number of slightly excited states. Because the total energy, and electronic structure of these states differ very little (by fractional occupation numbers only), we feel confident to stop the search for the true ground state at some computationally reasonable point.

Second, a cluster "density of states" (DOS) can be constructed by using Gaussian broadening functions; it shows the typical metallic fingerprint of a contracted d band slightly overlapping a diffuse s band. The HOMO–LUMO gap falls near the top of the d band. The s band, however, does show the previously mentioned unrealistic oscillations, as the distribution of the s states is simply too sparse in energy.

Third, the individual crystal orbitals of the cluster are delocalized over the entire cluster, as are true crystal orbitals of a bulk metal, rather than localized on specific atomic centra. All in all, the bare nine-atom cluster seems to provide an adequate representation of a metallic surface, although we must remain cautious so as not to overextend our conclusions. Naturally, the best test for cluster size would be to compare the adsorption characteristics of the nine-atom clusters to larger ones. However, we may already expect oscillations to occur in this size range, as they were observed in the binding energy of oxygen to $Ag_n$, $n = 4$, 10, 24, clusters [9a]. On the other hand, results of different calculations on a single cluster size can be compared among each other, to give reliable trends in adsorption characteristics.

## 3. Surface and subsurface carbon

As no structural data is available on the Co(0001)–C system, the carbon-to-surface spacing for the surface carbidic site was chosen to be 1.00

Å, as the Co–C distance of 1.76 Å is reasonable in light of the Ni–C distances calculated for hexagonal Ni(111) [12]. The subsurface site is modelled by placing the carbon in the octahedral hole midway between the first and second Co layers ($z = -1.018$ Å). Both sites are shown in fig. 1. The calculated ground state binding energies of the carbon atom to the Co cluster are nearly identical, 0.103 eV greater for the subsurface ($10(a_1)^2\ 11(a_1)^1\ 4(a_2)^2\ 14(e)^2$) than for the surface site ($11(a_1)^2\ 4(a_2)^2\ 5(a_2)^1\ 13(e)^2\ 14(e)^{0.5}\ 15(e)^{0.5}\ 16(e)^{0.25}$). Thus there appears to be no thermodynamic preference for the formation of one species over the other. Note that the absolute values of the binding energies are likely to be overestimated, a well-known shortcoming of the HFS–DVM methodology.

In addition to the octahedral subsurface site, we have also considered the tetrahedral site. Note that for a (0001) surface of a hcp metal, half of the potential sites between the layers are octahedral, the other half are tetrahedral. To model the tetrahedral site, one second layer Co was placed directly under the three-fold hollow, and the six neighboring Co's in that layer were added, in place of the three second layer Co's shown in fig. 1. The binding energy of carbon in this tetrahedral site is 4.12 eV less than in the octahedral model, thus the carbon binding energy is reduced by nearly half. That a carbon atom will bind less favorably in a tetrahedral position in the close-packed face is expected for a number of reasons. First, a literature search of binary metal carbides ($M_xC_y$) revealed no examples of tetrahedrally coordinated carbon centers. Second, organometallic complexes containing an encapsulated carbon species are typically at least eight-fold coordinated. Third, the Co–C distance at the tetrahedral site is only 1.517 Å, whereas even that of the octahedral site is short at 1.752 Å in comparison to the typical range of 1.95 to 2.10 found in metal carbides. Thus, we may expect tetrahedral sites in the Co(0001) surface to be filled after the octahedral ones, if at all. The remainder of our discussion will center about the octahedral carbon subsurface sites.

The Ziegler transition state method [13] can be used to split the binding energy into a repulsive term due to steric interaction ($E_{\text{steric}}$) and an attractive term due to stabilization of the electronic levels ($E_{\text{orb}}$). The electronic term can be further decomposed into the contribution by orbital symmetry type. Energy breakdowns are listed in table 2 ($1.00s^{GS}$ and $-1.018$ Å). That the binding energy of the two carbon sites is nearly identical appears to be due to a balance of steric and electronic factors. The steric repulsion experienced by the subsurface carbon is much greater than that of the surface carbon; however, the electronic stabilization is greater. The stabilization from the e states (C $2p_x$, $p_y$) is slightly more than that of the $a_1$ states (C 2s and $2p_z$). One could say that the somewhat "too tight" environment of the subsurface species is compensated for by the better overlap of electronic levels it provides.

Interesting to note is the rehybridization of the carbon atom. Fig. 2 shows the projected (or local)

Table 2
Binding energy breakdown in eV: carbon on $Co_9$ cluster (Electronic configuration = $10(a_1)^2\ 11(a_1)^1\ 4(a_2)^2\ 14(e)^2$)

| Carbon depth (Å) | $E_{\text{steric}}$ | Orbital interactions | | | | Binding energy |
|---|---|---|---|---|---|---|
| | | $E(a_1)$ | $E(a_2)$ | $E(e)$ | $E_{\text{orb}}$ | |
| 1.00 [GS] | 17.78 | −10.08 | −1.89 | −15.42 | −27.39 | −9.26 |
| 1.00 | 17.78 | −6.38 | −0.20 | −20.21 | −26.79 | −9.03 |
| 0.50 | 34.54 | −12.29 | −0.42 | −29.07 | −41.79 | −7.24 |
| 0.00 | 46.65 | −16.10 | −0.45 | −34.44 | −50.98 | −4.33 |
| 0.00 [R] | 40.58 | −14.37 | −0.30 | −32.34 | −47.01 | −6.43 |
| −0.429 | 43.40 | −16.44 | −0.23 | −32.67 | −49.23 | −5.94 |
| −1.018 | 35.55 | −16.04 | −0.07 | −29.16 | −45.27 | −9.72 |

[GS] Ground state configuration, $11(a_1)^2\ 4(a_2)^2\ 5(a_2)^1\ 13(e)^2\ 14(e)^{0.5}\ 15(e)^{0.5}\ 16(e)^{0.25}$.
[R] Relaxed cluster.

DOS of the carbon $2p_z$ (magnified $20\times$) and degenerate $2p_x$, $p_y$ pair ($10\times$) for the surface and subsurface sites. The respective total DOS's are provided for reference. The 2p levels are clearly different from each other at the surface site. The main peak of the surface C $p_x$, $p_y$ peak at $-7.8$ eV is shifted down from the $p_z$ peak at $-7.2$ eV. This is indicative of a more strongly bonding cluster–$p_x$, $p_y$ than $p_z$ interaction. Evidence of strong s–$p_z$ mixing is found in the concentration of $p_z$ density in the main C 2s peak at $-14.2$ eV (2s projection is not shown). The region is cluster–sp bonding; the antibonding counterpart, which is best described as an empty "lone pair" orbital pointing away from the surface, is pushed above the Fermi level. This orbital will be most important in the subsequent hydrogenation of the carbidic carbon. The parallel $p_x$, $p_y$–s mixing is not observed. The electronic environment of surface carbon can be thought of as analogous to molecular ammonia; bonding to the surface is tetrahedral, and reactivity is due to the fact that in this case, an empty s–$p_z$ orbital is pointing out of the surface. The description is verified by the contour plots in fig. 3 (taken along the $xz$-plane) of the electron density difference $\rho(Co_9C) - \rho(Co_9) - \rho(C)$. Both the C $p_x$, $p_y$ and the s–$p_z$ lobes pointing into the cluster gain electrons (solid line region) in forming the cluster–C bond, and the s–$p_z$ lobe point outwards is depleted (dashed line region). The PDOS's of

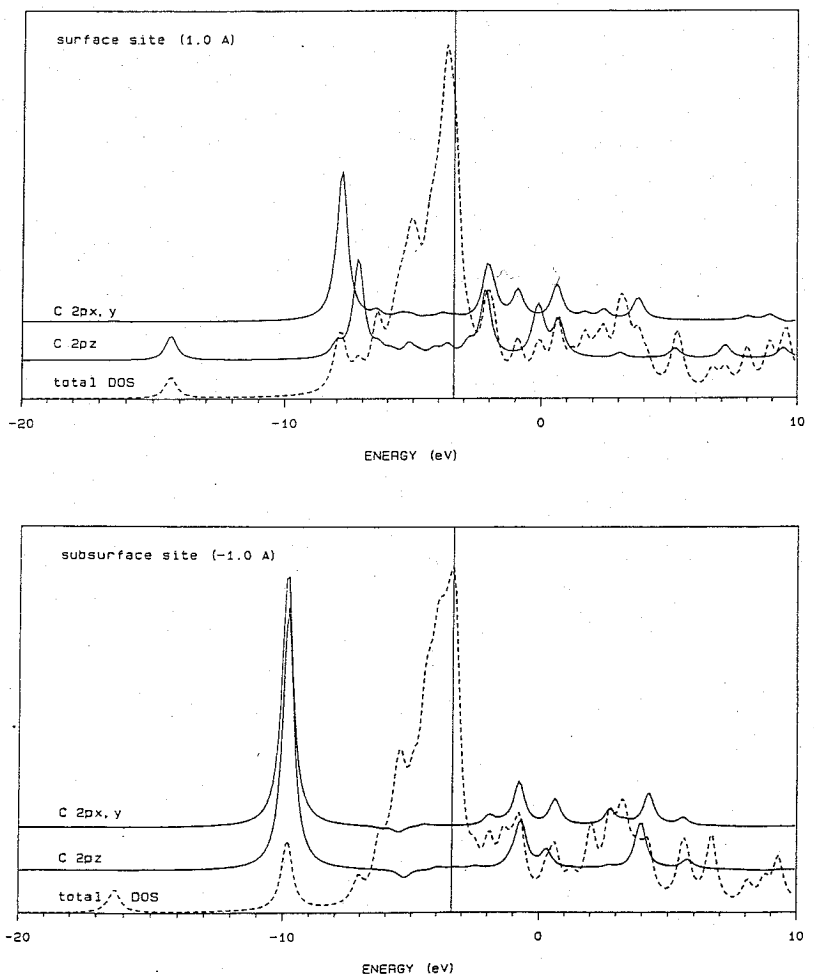


Fig. 2. Magnified projected DOS of C $2p_z$ ($20\times$) and $2p_x$, $p_y$ ($10\times$), and total DOS (dashed line) for $Co_9C$ clusters with C at $z = 1.0$ Å, surface site (upper panel) and $-1.018$ Å, subsurface site (lower panel). The Fermi level is indicated with a vertical line.

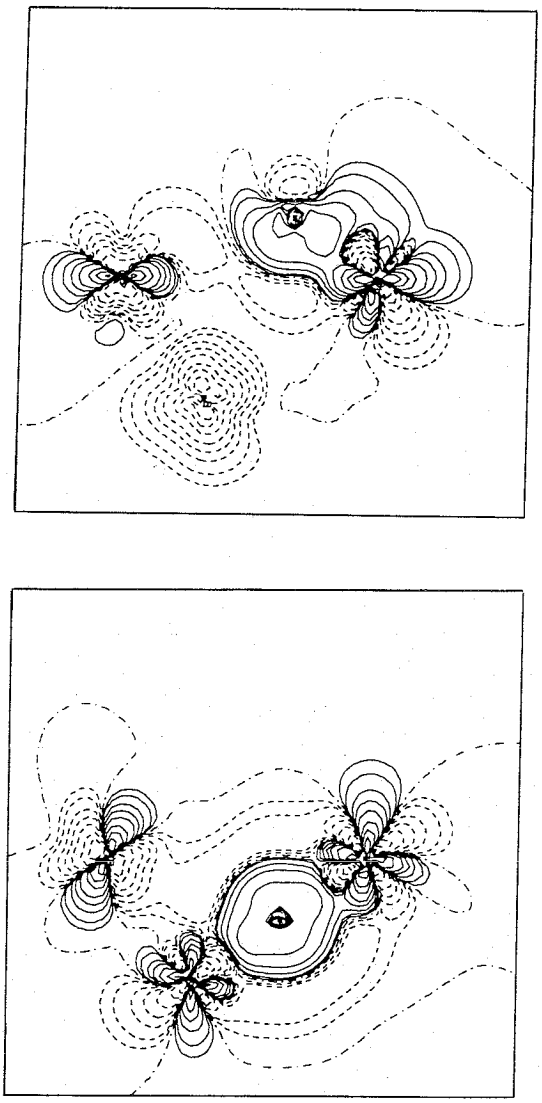

Fig. 3. Contour plots in the $xz$-plane of the electron density difference $\rho(Co_9C)\ \rho(Co_9) - \rho(C)$ with C at $z = 1.0$ Å, surface site (upper panel) and $-1.018$ Å, subsurface site (lower panel). Dashed lines show a decrease, solid lines an increase and dash-dot lines a nodal surface. Contours correspond to 0 $\pm 0.001$ $\pm 0.002$ $\pm 0.005$ $\pm 0.01$ $\pm 0.02$ $\pm 0.05$ $\pm 0.1$ $\pm 0.2$ and $\pm 0.5$ electrons/$a_0^3$.

fig. 2 are very similar to those obtained by self-consistent LCAO calculations [14] for carbidic films on 11 layer Ru(0001) and Rh(111) slabs, indicating that the finite cluster calculations can be used to build a reasonable descriptive analysis of the bonding.

The PDOS's of the subsurface carbon shown in fig. 2b indicates that the C 2p levels have become essentially degenerate, forming a strongly cluster bonding peak at $-9.9$ eV. No mixing is found with the C 2s level at $-16.4$ eV. In addition, the shape of the 2s level (not shown) remains relatively unchanged between the sites, with $\sim 80\%$ of the 2s density remaining in the main peak. That the electronic stablilization at the subsurface site is greater than at the surface site is seen in the strong downwards shift of all of the main carbon peaks. The electronic structure of the subsurface carbon is nearly circularly symmetric according to the electron density difference map in fig. 3b.

The rehybridization can also be tracked in the calculated carbon valence level electron occupations. The most strongly affected is the $2p_z$ level, gaining 0.38 $e^-$ from surface to subsurface sites. The $2p_x$, $p_y$ pair gains 0.27 $e^-$ each, and the 2s level loses 0.07 $e^-$. The net charge on the carbon atom increases from $-0.532$ $e^-$ to $-1.280$ [15].

To study the barrier between surface and subsurface sites, we have considered a five step path. The carbon atom is placed successively at $z = 1.00$ surface), 0.50, 0.0, $-0.429$ and $-1.018$ Å (subsurface). The test electronic state was fixed as that of the subsurface ground state, being the overall lowest energy state. The total energies so calculated will naturally lie above the individual ground states, and the energetic barrier we calculate represents a "worst case". The barrier is large, 4.70 eV. The energy breakdown in table 2 pinpoints the problem: a large steric repulsion as the carbon atom passes through the first layer. The C–Co distance is only 1.45 Å at this point. The path is clearly unrealistic.

Some information can be gained by examining the PDOS of the carbon levels along the path. As the carbon atom sinks, the majority $2p_z$ peak becomes larger and lowers in energy. Both effects result from the increasing cluster–C $2p_z$ interaction. Beyond $z = -0.429$ Å, the $2p_z$ peak is coincident with the $2p_x$, $p_y$ pair. The mixing with 2s disappears nearly completely when the carbon is level with the surface, indicating that its reactivity towards hydrogenation is nearly zero at this point. The main $2p_x$, $p_y$ and 2s peaks shift smoothly downwards in energy along the path, but their

Table 3
Net atomic charges: carbon on $Co_9$ cluster

| Carbon depth (Å) | Carbon | Co(1) | Co(2) | Co(3) |
|---|---|---|---|---|
| 1.00 | −0.532 | 0.131 | 0.065 | −0.019 |
| 0.50 | −0.835 | 0.231 | 0.038 | 0.009 |
| 0.00 | −1.051 | 0.328 | 0.009 | 0.013 |
| 0.00 [R] | −1.057 | 0.343 | 0.013 | −0.004 |
| −0.429 | −1.230 | 0.367 | 0.013 | 0.030 |
| −1.018 | −1.280 | 0.312 | 0.016 | 0.197 |

[R] Relaxed cluster.

PDOS's experience little change in overall shape.

Charging effects are of primary importance in the investigation of the poisoning or promoting characteristics of adatoms in general. If we consider the process of CO adsorption and dissociation, it is clear that electronegative adatoms will generally decrease the backbonding capacity of a metal, and poison CO dissociation. The $Co_9C$ clusters are too small to test the effect on CO adsorption directly, as the ratio of metal to nonmetal would become unrealistically high. However, an analysis of the electronic shifts of the metal levels in the $Co_9C$ clusters can give an indication of the effect on potential CO adsorption.

The charge transfer effect of the carbon on the metal cluster appears quite localized. Table 3 lists the net atomic charges. In all cases, the greatest charge transfer occurs at Co(1). For the surface carbon model, Co(1) loses twice as much as Co(2). For the subsurface carbon site, $d$(C–Co(1)) = $d$(C–Co(3)), so these cobalt atoms experience more nearly equal charge losses. Note that the electron loss from the surface atoms is greatest, thus the poisoning capacity is strongest, when the carbon atom is slightly *below* the surface (−0.429 Å). In this geometry, the charge loss from Co(2) is nearly 30 times less than that from Co(1).

However, analysis of the *net* charge transfer is perhaps not as important in determining the poisoning capacity of a species as the *relative* charge transfer induced between the various orbitals of one metal atom. As the deformation of the electron density about Co(1) is nearly identical, whether C is at −0.429 or at −1.018 Å, the density difference map of fig. 3b can be employed to analyze the effect of maximal poisoning on specific cobalt orbitals. The $d_{z^2}$ orbitals of both Co(1) and Co(2) gain electron density whereas the $d_{xz}$ orbitals lose density. The $d_{xz}$ orbitals point directly at the subsurface carbon center, so it is to be expected that they are most affected by the electron-withdrawing power of the carbon atom. If CO were to adsorb at either site, the $d_{z^2}$ orbital will be less able to accept electrons from the CO 5σ, thus the metal–CO bonding will weaken. The $d_{xz}$ orbital will, in turn, be less able to backdonate into the Co 2π, resulting in additional metal–CO bond weakening as well as reduced C–O bond weakening. The net result is that the presence of subsurface carbon is likely to reduce both CO adsorption and dissociation processes on nearby metal surface atoms.

These results are in general agreement with self-consistent surface linearized augmented plane wave (SLAPW) calculations of sulfur atoms adsorbed on a Rh(001) slab [16]. The net charge transfer to second-nearest neighbor metal atoms is negligible; however, rehybridization reduces the local DOS at the Fermi level. It was proposed that this reduction in the DOS may be responsible for the long-range poisoning effect of sulfur adatoms.

Recent electron density calculations of Darling et al. [12b] suggest that electron-withdrawing adatoms will force carbon atoms into the surface. This would indicate that the conversion of surface to subsurface carbon may be "self-catalyzing": the more subsurface carbon, the greater the extent of electron withdrawal, and thus the more carbon atoms are driven into the surface.

## 4. Surface relaxation

Up unto this point we have unjustly treated the metal lattice as a rigid, inflexible framework. Metal–metal bonding depends heavily on direction unspecified s–s interactions. This type of interaction can be described as "soft" small changes in the interatomic distances will cost little energy. The phenomena of phonon modes, surface relaxation and reconstruction are familiar conse-

quences. An adsorbed atom experiences a soft, mobile lattice enviroment, rather than a rigid network. In addition, the strong charge polarization brought upon by the burrowing carbon atom may act as the driving force for a surface reconstruction. As the steric repulsion between metal and carbon atom reaches a maximum at $z = 0.0$ Å, one can imagine that some stretching of the three-fold metal hollow may be induced, or that the barrier may be reduced by particular phonon modes.

In this light, we next consider a small perturbation to the Co(0001) metal framework. The surface atoms surrounding the three-fold hollow, Co(1), are allowed to relax outwards by 0.05 Å. As expected, the energetic price for performing the distortion is low, 0.1 eV. Little change is observed in the electronic structure of the cluster; the shape of the total DOS remains nearly identical, the cluster orbitals retain their delocalized character, and the maximum net atomic charge is $-0.0096$ $e^-$ on Co(2). To test if the low energetic cost of this relaxation is due to the small cluster size, and the incomplete coordination shell about the Co(1)'s, the relaxation was replicated for a larger cluster. The two additional neighbor atoms of Co(1) lying in the top layer were added, with a net increase of six atoms. The coordination number of each Co(1) is thus increased from six to eight. The energetic cost of the same relaxation for the larger cluster is 0.02 eV, thus a comparable value in light of the cluster approximation. Further discussion centers about the nine atom Co clusters.

Reconsidering the $z = 0.0$ Å carbon position after relaxation of the cluster, we find that the barrier to sinking is reduced by nearly half, to 2.60 eV (see table 2, $0.00^R$). The increase in Co–C distance is only 3.5%. The energy reduction is a result of a 6.07 eV lowering of the steric repulsion counteracted by a 3.97 eV decrease in the electronic stabilization.

Compared to the "soft" metal–metal interaction, the metal–carbon interaction can be considered "hard". The total energy is highly dependent on the carbon–metal distance. On an interatomic potential energy curve, the Co–Co interaction lies near the bottom of the energy well, and changes in distance have little effect on energy. The C–Co distance, on the other hand, is too short, lying on the repulsive slope. Small changes in distance have a much greater impact on the energy.

In fact, the calculated barrier is still unrealistically high. Using the effective medium approach, Chakraborty et al. [17] have examined the effect of lattice fluctuations in Ni(111) on the barrier between surface and subsurface sites of atomic oxygen. In the static limit, the barrier is 4.47 eV, comparable to our result of 4.70 eV. Allowing only thermally activated phonon modes, a barrier reduction to 0.41 eV with a 10% outwards distortion of the nickel three-fold site was found. If we allow for a similar relaxation in the $Co_9$ cluster with carbon at $z = 0.0$ Å, our barrier is now reduced to 0.49 eV, again in excellent agreement with the O–Ni(111) results. Two important facts emerge: (1) in this study, an LDA cluster approximation produces results in very close agreement to a semi-empirical extended structure method, and (2) a small, energetically inexpensive, and perhaps even thermally activated relaxation of the metal lattice can greatly reduce the barrier to sinking. Thus the formation of subsurface carbon from surface adatom species appears an amenable process. If surface carbon atoms are evident, one must seriously consider the occurrence of subsurface carbon as well.

There is an interesting parallel between these results and the multireference CCI calculations on $Ni_5C$, $Ni_5N$ and $Ni_5O$ of Seigbahn et al. [18]. If relaxation of the nickel cluster is allowed, they find that all of the adsorbates penetrate the surface to a depth of $0.42 \pm 0.16$ Å in their lowest energy position. However, if cluster relaxation is *not* allowed, the adsorbates all remain $1.11 \pm 0.11$ Å above the surface. Thus both the HFS–$X\alpha$ and multireference CCI calculations find surface relaxation paramount to the creation of subsurface species.

## 5. Effect of atomic oxygen

Although oxygen is quickly removed from the surface after CO dissociation under catalytic conditions, it is interesting to consider the effect of nearby surface oxygen atom on the conversion of surface to subsurface carbon. If indeed nearby

oxygen aids the process, the lifetime of oxygen atoms on the surface may be an important parameter. Although a very different surface from Co(0001), it has been found that oxygen adsorption induces subsurface carbon formation on carbon-covered W(001) [19].

Surface atomic oxygen was modelled by placing three oxygen atoms 1.0 Å above three-fold hollow positions directly above the second layer Co(3) atoms. The binding energy is very favorable: −25.55 eV. Subsequently, a carbon atom is placed at the surface carbidic position, at $z = 0.0$ Å, and in the subsurface site. Of the three, only the binding energy of the subsurface carbon (relative to the oxidized cluster) is attractive, BE = −8.12 eV. However, in comparison to the cluster without oxygen, the binding energy is reduced by 1.6 eV. The surface carbidic site becomes repulsive (BE = +0.56 eV) in the presence of surface oxygen, and the $z = 0.0$ Å even more so (BE = +2.97 eV). From this three step path, the barrier to conversion from surface to subsurface sites on the oxidized surface can be estimated at 2.41 eV, and is thus even less than in the case of the relaxed, unoxidized cobalt cluster.

Neighboring oxygen induces a strong preference of subsurface over surface carbon species. The observed extreme repulsive behavior of the surface carbon atom in an oxidized environment may well be a function of improper modelling. Using a larger metal cluster would reduce the unrealistic adsorbate : substrate ratio of 4 : 9, unfortunately at a rather high computational price.

## 6. Conclusions

Our HFS–LCAO calculations suggest that surface relaxation is crucial to the formation of subsurface carbon species. The computed barrier for movement of a carbon atom from a surface carbidic site to a subsurface site is reduced by 50%, if a small relaxation (1% outwards displacement) is allowed to take place. Indeed, by analogy to Ni(111) effective medium calculations, a 10% relaxation of the lattice may be thermally allowed. In this case, a barrier reduction of ~ 90%, to 0.49 eV, is computed. Note that, the path we have chosen can be regarded as a "worst case", as (1) surfaces other than (0001) have either steps or hollows larger than three-fold, and (2) we have not taken the ground electronic state at each point along the reaction path, but rather, have fixed the electronic configuration at that of the most stable final state.

Two important questions now arise. First, what is the consequence of the formation of subsurface carbon on reactions such as the Fischer–Tropsch process? The modification of the surface electronic structure appears very local, being restricted to only the immediately neighboring metal atoms. To properly answer this question, one must either move to larger clusters or perform slab calculations. Second, and most importantly, can such species be detected by experimental techniques? Work continues in both areas.

## Acknowledgements

M.C.Z. is grateful to Professor E.J. Baerends and P. Vernooijs of the Free University of Amsterdam for their helpful advice and discussions, and to the referees for the careful reading of the manuscript.

## References

[1] (a) R.W. Joyner and M.W. Roberts, J. Chem. Soc. Faraday Trans. I, 70 (1974) 1819;
(b) R.W. Joyner, Surf. Sci. 63 (1976) 291;
(c) J. Nakamura, I. Toyoshima and K. Tanaka, Surf. Sci. 201 (1988) 185.

[2] (a) D.W. Goodman, Acc. Chem. Res. 17 (1984) 194, and refences therein;
(b) D.W. Goodman, R.D. Kelley, T.E. Madey and J.T. Yates, Jr., J. Catal. 63 (1980) 226.

[3] R.W. Joyner, G.R. Darling and J.B. Pendry, Surf. Sci. 205 (1988) 513.

[4] G.F. Raupp and W.N. Delgass, J. Catal. 53 (1979) 348, 361;
M.E. Dry, Catalysis and Technology (Springer, Berlin, 1983) p. 161.

[5] S. Nagakura, J. Phys. Soc. Jpn. 12 (1957) 482;
L.J.E. Hofer and W.C. Peebles, J. Am. Chem. Soc. 69 (1947) 893.

[6] J.C. Hamilton and J.M. Blakely, Surf. Sci. 91 (1980) 199;
J.F. Mojica and L.L. Levenson, Surf. Sci. 59 (1976) 447.

[7] (a) J.J.C. Geerlings, M.C. Zonnevylle and C.F.M. de Groot, Catal. Lett. 5 (1990) 309;
(b) J.J.C. Geerlings, M.C. Zonnevylle and C.F.M. de Groot, Surf. Sci., submitted.
[8] E.J. Baerends, D.E. Ellis and P. Ros, Chem. Phys. 2 (1972) 41.
[9] (a) P.J. van den Hoek, E.J. Baerends and R.A. van Santen, J. Phys. Chem. 93 (1989) 6469;
(b) A.P.J. Jansen and R.A. van Santen, J. Phys. Chem. submitted;
(c) D.E. Ellis, J. Guo and H.P. Cheng, J. Phys. Chem. 92 (1988) 3024.
[10] J.G. Snijders, F. Vernooijs and E.J. Baerends, At. Data Nucl. Data Tables 26 (1981) 483;
Internal Report Free University, Amsterdam, 1981, unpublished.
[11] D. Post and E.J. Baerends, J. Chem. Phys. 78 (1983) 5663; K. Hermann, P. Bagus and C. Nelin, Phys. Rev. B 26 (1987) 9467.
[12] (a) K.W. Jacobson and J.K. Nørskov, Surf. Sci. 166 (1986) 539;
(b) G.R. Darling, J.B. Pendry and R.W. Joyner, Surf. Sci. 211 (1989) 69.
[13] T. Ziegler and A. Rauk, Theoret. Chim. Acta 43 (1977) 1.
[14] P.J. Feibelman, Phys. Rev. B 26 (1982) 5347.
[15] Some electron transfer also occurs in the polarization functions.
[16] P.J. Feibelman and D.R. Hamann, Phys. Rev. Lett. 52 (1984) 61.
[17] B. Chakraborty, S. Holloway and J.K. Nørskov, Surf. Sci. 152 (1985) 660.
[18] I. Panas, J. Schüle, U. Brandmark, P. Seigbahn and U. Wahlgren, J. Phys. Chem. 92 (1988) 3079.
[19] D.R. Mullins and S.H. Overbury, Surf. Sci. 210 (1989) 501.